Computational Modeling of Vortex Ring State Modes
of Helicopter Main Rotor.

Ignatkin Y.M., Makeev P.V., Shomov A.I.
Moscow Aviation Institute
(National University of Science)
Russia

Abstract.

This work is concentrated on research of helicopters' main rotor aerodynamics at the vortex ring state modes.

At the basis of non-linear blade vortical model with free-wake the numerical computation of various modes of vertical descent including vortex ring state modes were performed. As a result the form of a rotor free-wake, velocity fields and airflow lines for the flow around the rotor were got. Components of the forces and of the moments acting on a rotor were also obtained. The problem of computational modeling of helicopters' main and tail rotors' aerodynamics at the vortex ring state mode was solved taking into account rotors' interference.

Finally the indication set of vortex ring state mode including rotors thrust pulsations, forms of a free wake and power increase in comparison with hover was got and analyzed.

NOMENCLATURE

T	- rotor trust, N;
Q	- rotor torque, N;
c_T	- rotor trust coefficient, $(2 \cdot T)/(\rho \cdot (\omega R^2) \cdot \pi R^2)$;
c_Q	- rotor torque coefficient, $(2 \cdot Q)/(\rho \cdot (\omega R^2) \cdot \pi R^3)$;
V_0	- flight velocity, m/s;
V_y	- climb velocity, m/s;
V_x	- horizontal velocity, m/s;
ωR	- rotary axis speed, m/s;
υ_i	- induced velocity (at a rotor disc plane);
υ_{ih}	- hover induced velocity, m/s; $\upsilon_{ih} = \omega R \cdot 0,5\sqrt{c_T}$
$\tilde{\upsilon}_y$	- non-dimensional induced velocity, υ_i/υ_{ih};
$\tilde{V}_0$	- non-dimensional flight velocity, V_0/υ_{ih}
$\alpha_H°$	- angle of rotor attack, degree;
$\varphi_7°$	- blade attack angle, degree;

$\Delta\varphi_\Sigma°$	- blade twist, degree;
$\psi°$	- azimuth angle, degree;
b	- rotor blade chord, m;
R	- rotor radius, m;
n_b	- number of blades;
σ	- rotor solidity, $n_b \cdot b/\pi R$;
ρ	- air density, kg/m^3;
Re	- Reynolds number
VRS	- vortex ring state;
FLH	- flapping hinge;
FTH	- feathering hinge;
CW	- clockwise;
CCW	- counterclockwise.

INTRODUCTION

Research of helicopter's main rotor's behavior on the descent with low speeds is really actual for providing safety and flight maneuverability. Such types of research, as a rule, require expensive and complicated experiments as well as they are connected with high risk flight tests.

Using of modern information technologies gives a chance to implement numerical (mathematical) models, able to

reflect precisely enough real physical processes during the rotor's work. Application of such models allows to solve the problems of rotors aerodynamics modeling on the complicated working modes, which have not been available for complex modeling before.

The task is solved through using of non-linear blade vortical model of helicopter rotor and its software realization created by authors at the Moscow Aviation Institute (National University of Science) [Ref. 1, 2].

The considered cases include:
- descent with low speeds (vortex ring state modes) of helicopter's main rotor.
- work of tail rotor in free-wake of main rotor at the vortex ring state mode.

Main and tail rotors of single-rotor classical helicopter scheme were considered as a subject of the research.

THE VORTEX RING STATE MODE OF HELICOPTER'S MAIN ROTOR

The vortex ring state mode of helicopter's rotor appears in the process of helicopter's steep descent with low speeds. Flow velocity being thrown by rotor in this case becomes close to velocity of flow arriving to the rotor. Free vertical wake does not move away from rotor disk plane, making near it circulating motions and creating vertical structure similar to vortex ring (Fig. 1).

Computational and experimental researches show that vortex wake at these modes is characterized by extreme complexity [Ref. 4-14]. Not only external vortex ring created by rolling up free vortex wake, which runs from bled end part, forms rotor's flowing. In addition to external ring internal vortex ring is made by free vortexes which run from root blade parts.

Interference of both vortex rings together with creating secondary circulation areas, discreteness of free vortex wake, blade flapping, wake diffusion in strongly turbulized airflow- not only these factors determine the rotor flowing and time changing of rotor's aerodynamic characteristics at the vortex ring state mode.
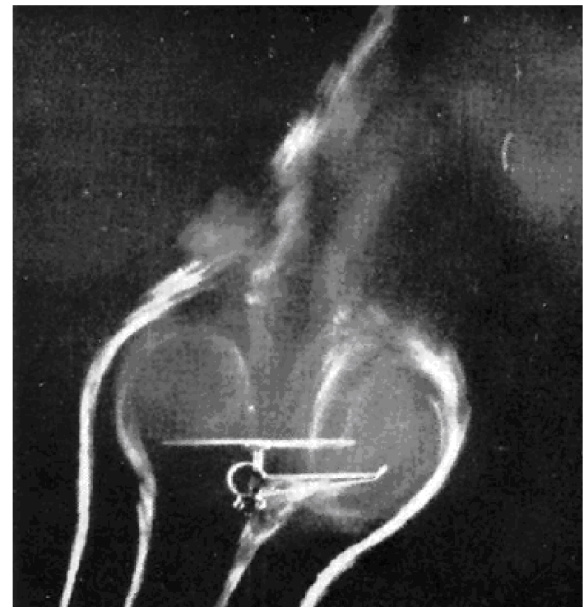

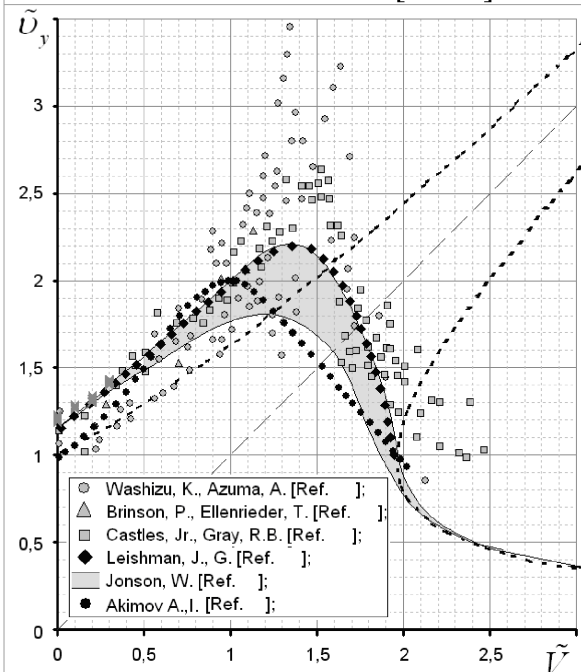**Fig. 1.** Experimental visualization of vortical wake at VRS [Ref. 8].

Fig. 2. Experimental diagrams of $\tilde{\upsilon} = f(\tilde{V})$ dependences.

In results of flight and wind tunnel tests [Ref. 3, 9-14] at the vortex ring state mode there are:
- rotor trust pulsation;

- oscillation of rotary axis speed (ωR) due to changing of rotor torque during the time;
- spontaneous surges of course, list and pitch;
- increase of necessary control on all channels including altitude;
- high vibration of helicopter with unsteady frequency;
- blade cone oscillation with rotor's forces and moments changing during the time.

The results of experimental (wind tunnel) research of vortex ring state modes usually are represented by dependence of non-dimensional induced velocity at a rotor disk plane $\tilde{\upsilon}_y$ on non-dimensional flight velocity $\tilde{V}$ for various angles of rotor attack α_H.

Fig. 2 represents results of experimental research for the angle of rotor attack α_H =90° [Ref. 3, 9-13].

Results above were received for concrete rotors with characteristics given and have essential difference. This fact is connected, firstly, with various rotors' geometry and, secondly, with oscillation of rotor torque and trust due to unsteady rotor flowing. Besides this, type of flowing of rotor blades at the vortex ring state mode most of all depends on air viscosity, which is connected with Reynolds number and level of initial air turbulence. Additionally Reynolds number and level of initial air turbulence are different in wind tunnel and flight tests.

Circumstances mentioned above prove the necessity of making computational modeling of vortex ring state modes for concrete rotors with concrete geometric characteristics for real coefficients of rotor trust and Reynolds number.

NON-LINEAR BLADE VORTICAL MODEL OF ROTOR

Non-linear blade vortical model of rotor is the basis for computational modeling [Ref. 1]. In this model every blade is composed by lifting line and adjoined vortex is located on quarter of chord (Fig. 3). Rotor blade is modeled by set of plane rectangle elements. Rotor hub has flapping hinges relative to them blades make flapping motions and also hub has feathering hinges which allow changing blade pitch angles.

While the rotor is moving, blade generates the system of longitudinal and transversal vortexes, which are making free vortex wake (Fig. 3). The wake looks like a net made of vortex rectangles.

For calculation of aerodynamic characteristics hypothesis of plane section is used. Aerodynamic characteristics of airfoils are evaluated basing on the data of wind tunnel tests under relevant values of Re and M numbers.

In this model vortex segments of vortex wake grid are modeled by diffusing vortex lines. Taking into account the vortex diffusion allows to model physical processes at the vortex wake more precisely and to avoid producing mathematical peculiarities which lead to fast destroy of the grid.

To find the deformation of free vortex wake behind rotor blades it is necessary to evaluate induced velocities in grid points of all vortex segments in every moment. Non-linear free vortex wake behind the rotor is built step by step as a result of calculation.

Fig. 4 represents geometric model of main and tail rotor used in calculation.

Blade of main rotor was modeled by 12 elements and blade of tail rotor – by 10 elements. Azimuth angle of calculation step is $\Delta\psi°$=12°.

Main rotor parameters: n_b=3; R=7,25 m; σ=0,0527; ωR=187 m/s; $\Delta\varphi_\Sigma°$=-6°; blade airfoil NACA 230-12.

Tail rotor parameters: n_b=3; R=1,35 m, σ=0,0527; ωR=205 m/s; $\Delta\varphi_\Sigma°$=0; blade airfoil NACA 0012.
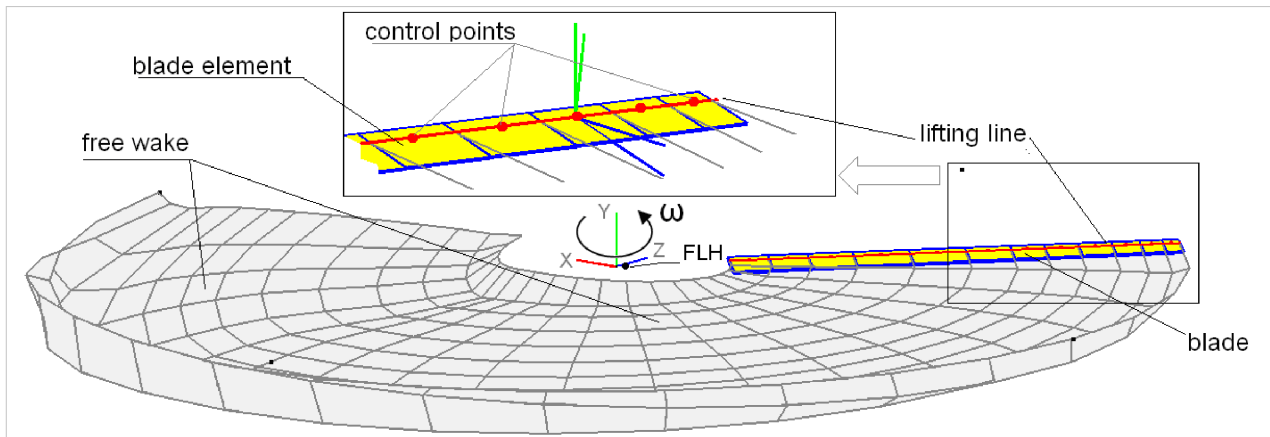
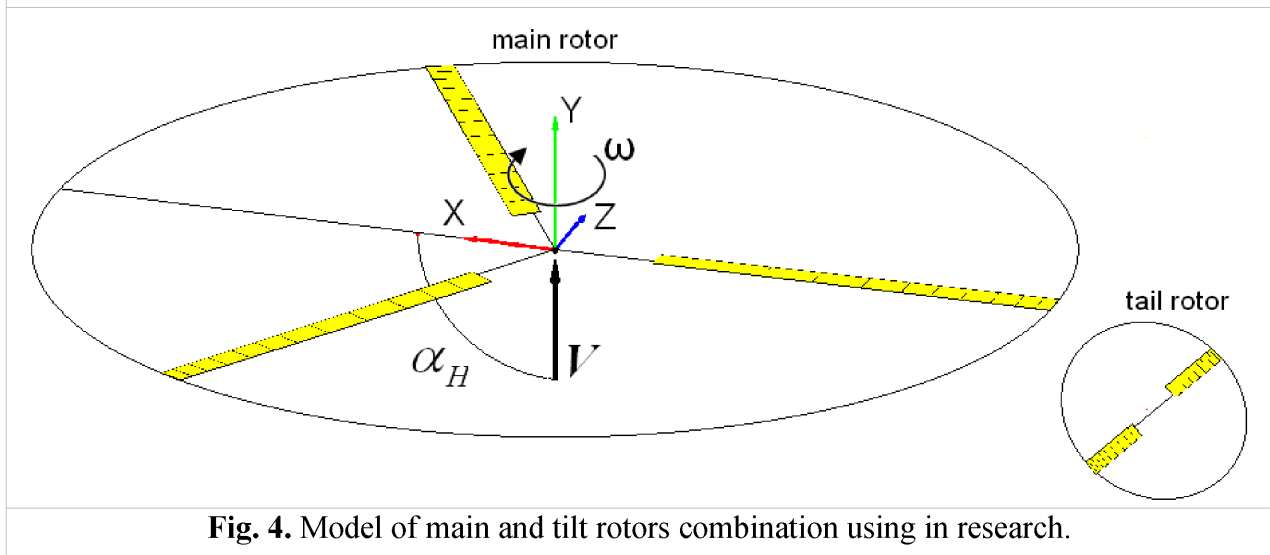**Fig. 3.** Non-linear blade vortical model of helicopter rotor (free-wake model).

Fig. 4. Model of main and tilt rotors combination using in research.

RESULTS OF CALCULATION OF MAIN ROTOR AERODYNAMIC CHARACTERISTICS AT DESCENT
$(\alpha_H = 90°)$

The calculation was made for a number of vertical descent speeds V_Y =0...20 m/s with step 1 m/s. Values of blade attack angle were chosen with the purpose of having constant mean value of main rotor trust coefficient for all flight regimes ($c_T \approx 0,01$). Calculation was made for main rotor revolution with n=18.

Rotor flowing visualization was made with the help of airflow lines constructed in the plane perpendicular to rotor disk plane. Such flowing visualization is the most convenient because of high complexity of free vortex wake form at the vortex ring state modes.

Aerodynamic characteristics are represented by dependences: $c_T, c_Q, \beta = f(n)$, $\tilde{\upsilon}_y = f(\tilde{V})$ and $c_Q / c_{Qh} = f(\tilde{V})$ for $\alpha_H = $ const.

Fig.5 demonstrates calculation data $\tilde{\upsilon}_y = f(\tilde{V})$ for $\alpha_H = 90°$.

It is seen that at every flight regime (with blade attack angle $\varphi_7°$ values given and descent speed V_Y) dependence of $\tilde{\upsilon}_y = f(\tilde{V})$ is ambiguous and defined by a number of values because of velocity pulsation $\tilde{\upsilon}_y$ and trust coefficient value c_T during the time. Thereby dependence of $\tilde{\upsilon}_y = f(\tilde{V})$ with $\alpha_H = $ const as a result of aerodynamic characteristics pulsations is represented not by a curve, but by value area

(Fig.5). Large solid points represent values $\tilde{\upsilon}_y\left(\tilde{V}\right)$ corresponding to average value of trust coefficient $c_T \approx 0{,}01$ given.

Maximum value of $\tilde{\upsilon}_y$ velocity with taking into account pulsation can be with $\tilde{V} \approx 0{,}9$ and is $\tilde{\upsilon}_y \approx 3{,}4$.

Maximum value of $\tilde{\upsilon}_y$ with average trust value ($c_T \approx 0{,}01$) is reached with $\tilde{V} \approx 0{,}8$ and it is $\tilde{\upsilon}_y \approx 2{,}9$.

Fig. 5 also demonstrates a curve $c_Q / c_{Qh} = f(\tilde{V})$ (with $c_T \approx 0{,}01$, without taking into account rotor torque pulsation). Graph shows that when descent speed increases growth of value c_Q reaches 65% (comparing with hover) with V_Y=7…8 m/s ($\tilde{V} \approx 0{,}8$). Then with descent speed increases torque coefficient decreases and reaches zero, when rotor is in autorotation.

Fig. 7…10 represent airflow lines and Fig.11…14 demonstrate dependences of aerodynamic characteristics on a number of rotor revolutions with $\alpha_H = 90°$ and V_Y=5,8,15,18 m/s.

Fig. 11 shows that at the hover (V=0) aerodynamic characteristics c_T, c_Q, β with n increasing remain constant. The same situation is with speeds up to V_Y=4 m/s.

With descent speed V_Y=5 m/s there come the first features of vortex ring, characterized by all aerodynamic characteristics pulsation during the time and firstly, trust coefficient pulsation c_T (see Fig. 12).

Aerodynamic characteristics changes during the time are explained by peculiarities of rotor flowing (see Fig. 7). Around the rotor 'air body' with upper and lower borders appears and airflow is not thrown off anymore, as at hover, but circulates through rotor disk plane (see Fig. 7). Vortex ring under the rotor is obviously seen.

When descent speed increases up to V_Y=8 m/s vortex ring is located in the centre relative to rotor disk plane (see Fig. 8). Trust coefficient pulsation c_T peaks up to $\delta c_T \approx 20\%$ (see Fig. 13), which complies with 'peak' of vortex ring state mode, velocity $\tilde{\upsilon}_y$ at this mode also was maximum (see Fig. 6).

Aerodynamic characteristics pulsations stop with descent speed V_Y=15 m/s (see Fig. 14), when rotor works in autorotation mode. "Air body' in this case moves up (see Fig. 9). When descent speed goes on increasing, rotor works as a windmill (see Fig. 10).
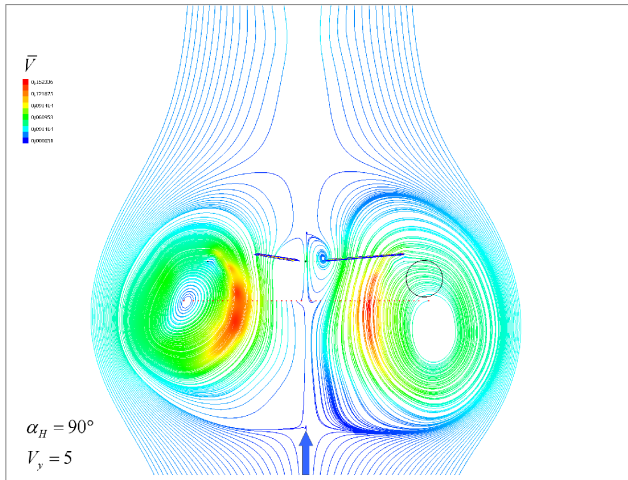

Fig. 6. Diagrams of $\tilde{\upsilon} = f\left(\tilde{V}\right)$ and $c_Q / c_{Qh} = f(\tilde{V})$ for $\alpha_H = 90°$.

Fig. 7. Airflow lines near main rotor at descent $\alpha_H = 90°$; $V_y = 5$ m/s.
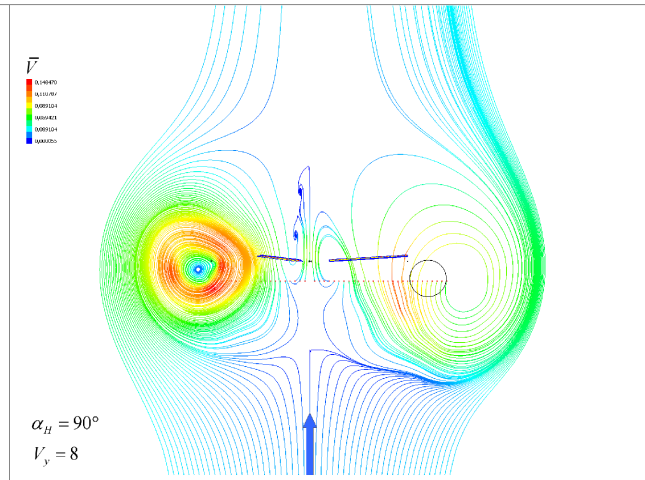

Fig. 8. Airflow lines near main rotor at descent $\alpha_H = 90°$; $V_y = 8$ m/s.
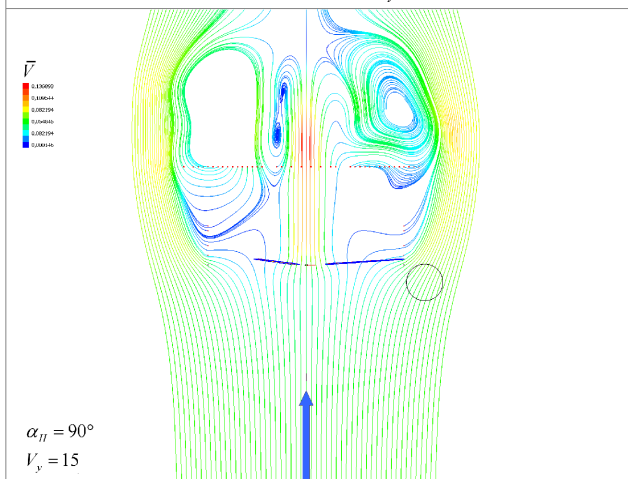

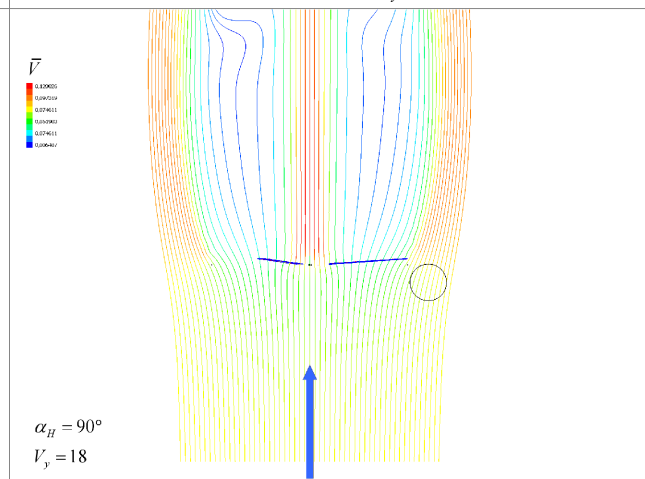**Fig. 9.** Airflow lines near main rotor at descent $\alpha_H = 90°$; $V_y = 15$ m/s.

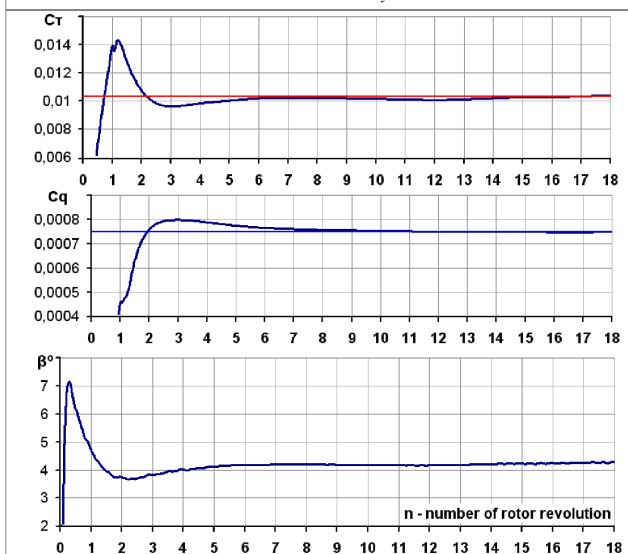**Fig. 10.** Airflow lines near main rotor at descent $\alpha_H = 90°$; $V_y = 18$ m/s.

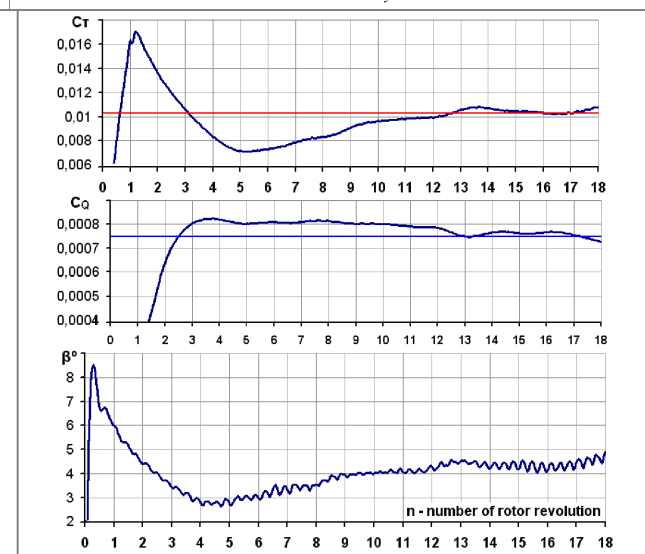**Fig. 11.** Coefficients Ct, Cq and blade flapping angle of main rotor at hover ($\alpha_H = 90°$; $V_y = 0$ m/s).

Fig. 12. Coefficients Ct, Cq and blade flapping angle of main rotor at descent ($\alpha_H = 90°$; $V_y = 5$ m/s).
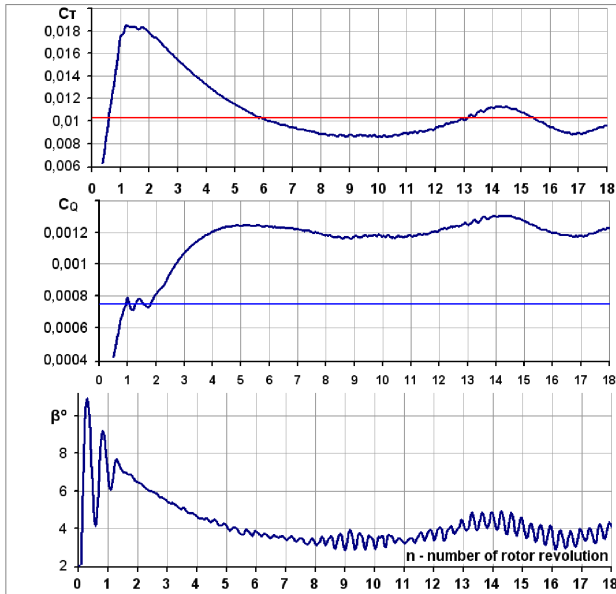
Fig. 13. Coefficients Ct, Cq and blade flapping angle of main rotor at descent ($\alpha_H = 90°$; $V_y = 8$ m/s).
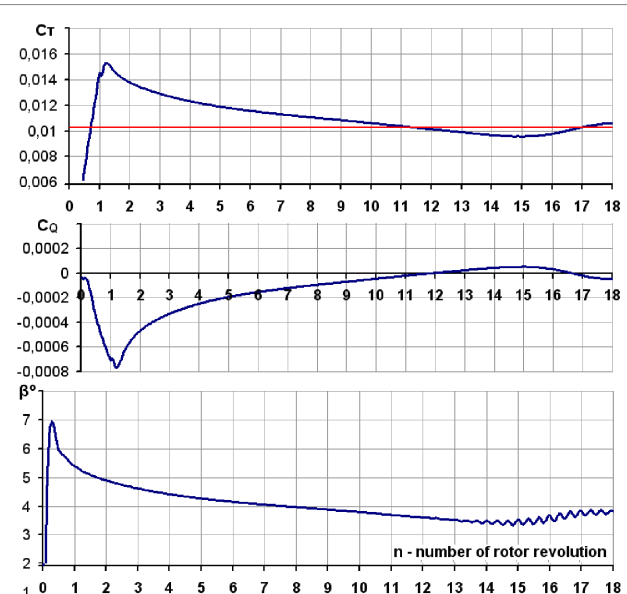

Fig. 14. Coefficients Ct, Cq and blade flapping angle of main rotor at descent ($\alpha_H = 90°$; $V_y = 15$ m/s).

RESULTS OF CALCULATION OF MAIN ROTOR AERODYNAMIC CHARACTERISTICS AT DESCENT ($\alpha_H = 70°$)

The calculation was made for a number of vertical descent speeds $V_Y = 0...18$ m/s with step 1 m/s. As for $\alpha_H = 90°$ values of blade attack angle were chosen with the purpose of having constant mean value of main rotor trust coefficient for all flight regimes ($c_T \approx 0,01$).

Fig. 15 demonstrates calculation data $\tilde{\upsilon}_y = f\left(\tilde{V}_y\right)$ for $\alpha_H = 70°$.

Maximum value of $\tilde{\upsilon}_y$ velocity with taking into account pulsation can be with $\tilde{V} \approx 0,8...0,9$ and is $\tilde{\upsilon}_y \approx 2,4$. Maximum value of $\tilde{\upsilon}_y$ with average trust value ($c_T \approx 0,01$) is reached with $\tilde{V} \approx 0,75$ and it is $\tilde{\upsilon}_y \approx 2$.

Fig. 15 demonstrates a curve $c_Q / c_{Qh} = f(\tilde{V}_y)$ (with $c_T \approx 0,01$, without taking into account rotor torque pulsation). Graph shows that when descent speed increases growth of value c_Q reaches 17% with $V_Y = 7$ m/s ($\tilde{V} \approx 0,75$). Then with descent speed increase torque coefficient decreases and reaches zero, when rotor is in autorotation. Fig. 16…19 represent airflow lines and Fig. 20…23 demonstrate dependences of aerodynamic characteristics on number of rotor revolutions with $\alpha_H = 70°$ and $V_Y = 4,7,13,16$ m/s.
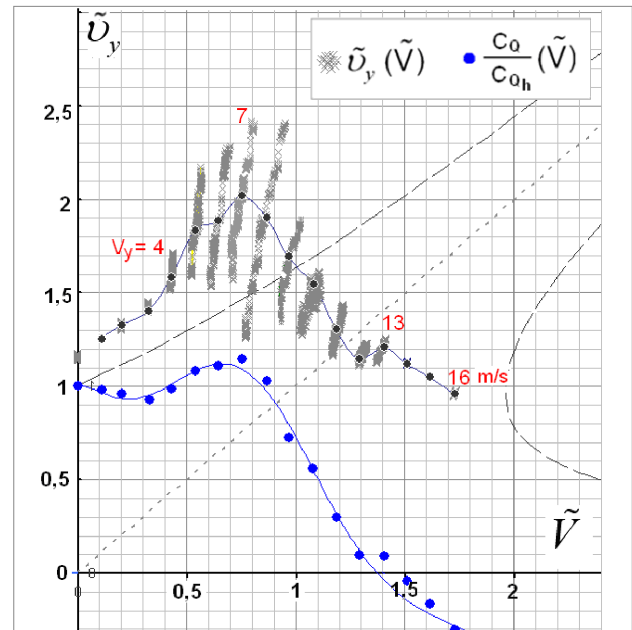

Fig. 15. Diagrams of $\tilde{\upsilon}_y = f\left(\tilde{V}\right)$ and $c_Q / c_{Qh} = f(\tilde{V})$ for $\alpha_H = 70°$.

Fig. 15 shows that aerodynamic characteristics c_T, c_Q, β with n increasing remain constant up to V_Y=3 m/s.

With descent speed V_Y=4 m/s there come the first features of vortex ring, characterized by all aerodynamic characteristics pulsation during the time and firstly, trust coefficient pulsation c_T (see Fig. 20).

Around the rotor 'air body' with upper and lower borders appears, as for $\alpha_H = 90°$, but as opposed to vertical descent 'air body' is asymmetric and is inclined by flow (see Fig. 16).

Trust coefficient pulsation c_T peaks with V_Y=7 m/s (see Fig. 17, 21), blade flapping and velocity $\tilde{v}_y$ at this mode also reach maximum. With V_Y=13 m/s 'air body' moves up (see Fig. 18), and aerodynamic characteristics pulsations almost stop (see Fig. 22), rotor moves into autorotation. When descent speed goes on increasing rotor works as a windmill (see Fig. 23).
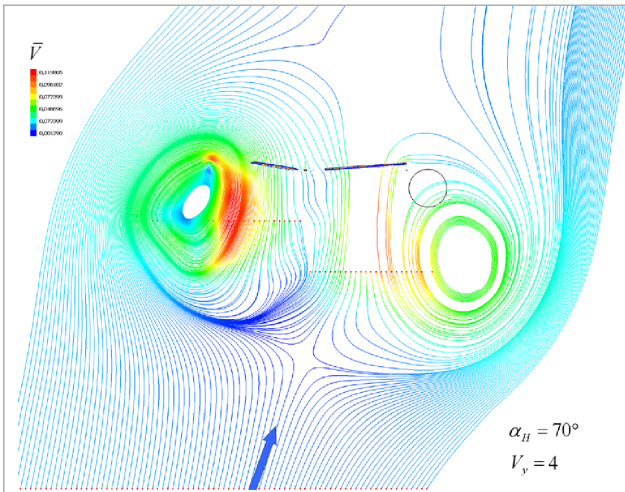

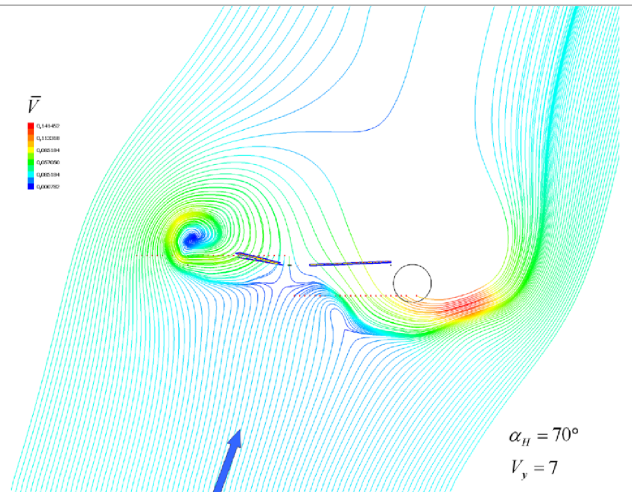**Fig. 16.** Airflow lines near main rotor at descent $\alpha_H = 70°$; $V_y = 4$ m/s.

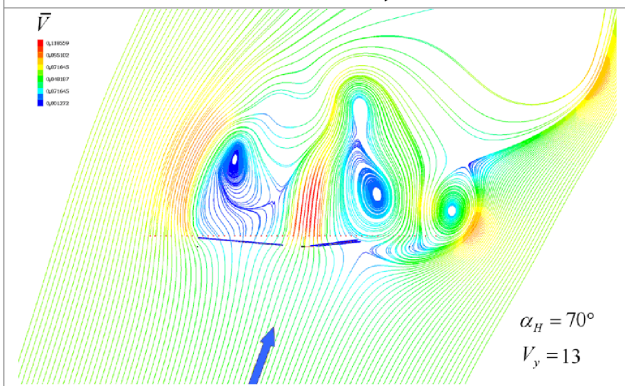**Fig. 17.** Airflow lines near main rotor at descent $\alpha_H = 70°$; $V_y = 7$ m/s.

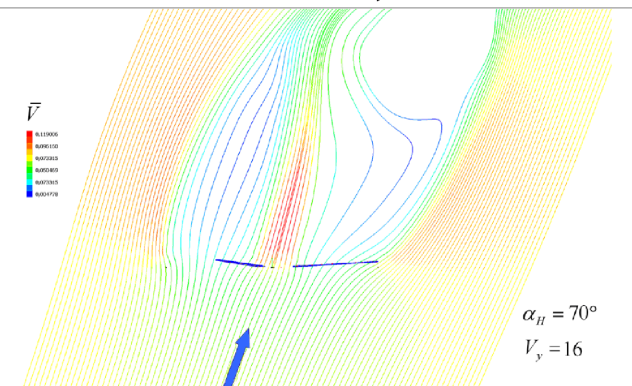**Fig. 18.** Airflow lines near main rotor at descent $\alpha_H = 70°$; $V_y = 13$ m/s.

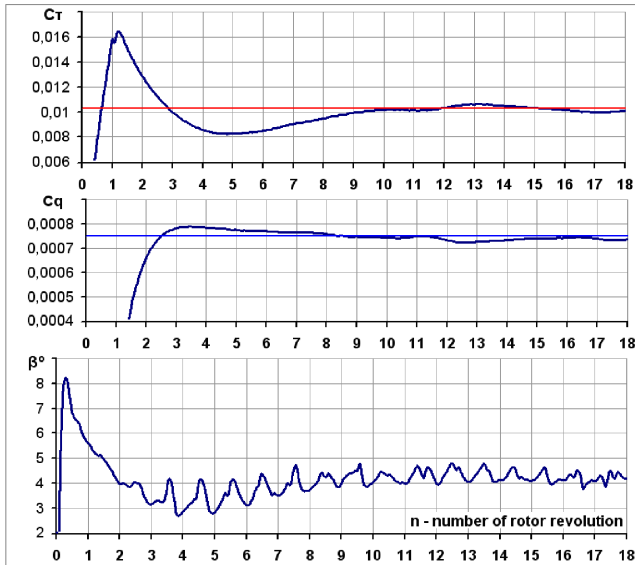**Fig. 19.** Airflow lines near main rotor at descent $\alpha_H = 70°$; $V_y = 16$ m/s.

Fig. 20. Coefficients Ct, Cq and blade flapping angle of main rotor at descent ($\alpha_H = 70°$; $V_y = 4$ m/s).
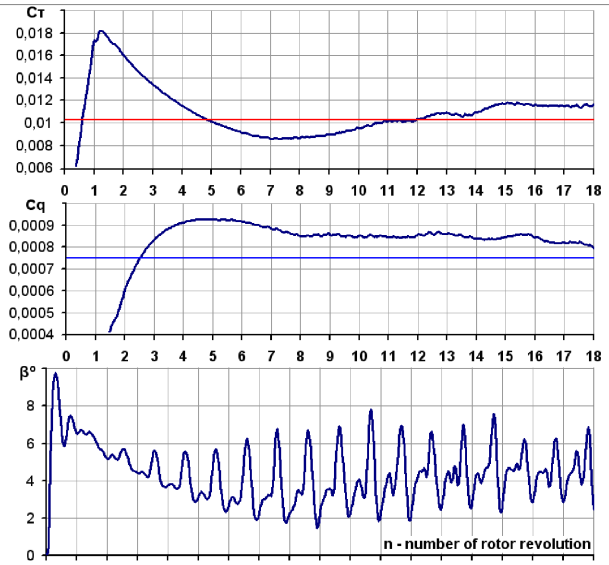

Fig. 21. Coefficients Ct, Cq and blade flapping angle of main rotor at descent ($\alpha_H = 70°$; $V_y = 7$ m/s).
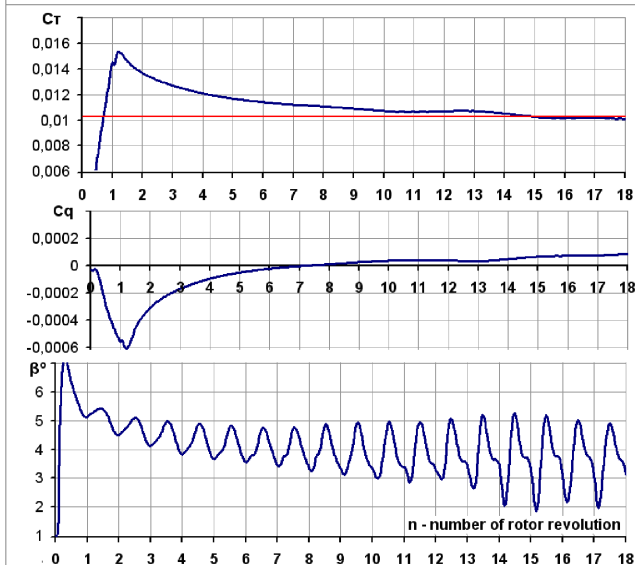

Fig. 22. Coefficients Ct, Cq and blade flapping angle of main rotor at descent ($\alpha_H = 70°$; $V_y = 13$ m/s).
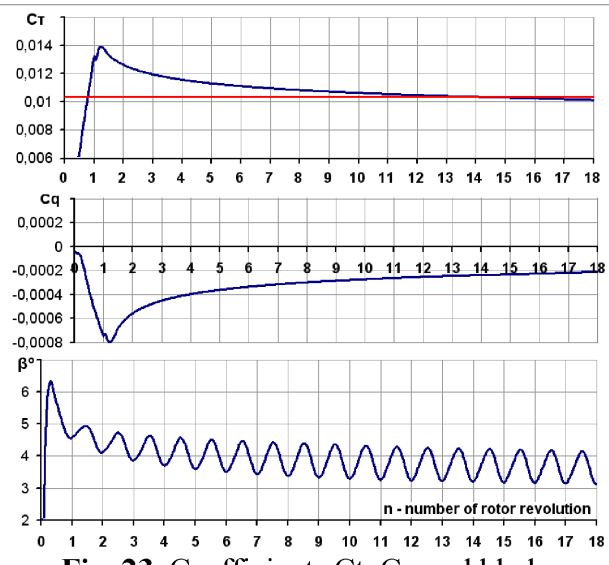

Fig. 23. Coefficients Ct, Cq and blade flapping angle of main rotor at descent ($\alpha_H = 70°$; $V_y = 16$ m/s).

RESULTS OF CALCULATION OF MAIN ROTOR AERODYNAMIC CHARACTERISTICS AT DESCENT ($\alpha_H = 30°$).

The calculation was made for a number of vertical descent speeds $V_Y = 0\dots12$ m/s with step 1 m/s. As for $\alpha_H = 90°$ and $\alpha_H = 70°$ values of blade attack angle were chosen with the purpose of having constant mean value of main rotor trust coefficient for all flight regimes ($c_T \approx 0,01$).

Fig. 24 demonstrates calculation data $\tilde{\upsilon}_y = f(\tilde{V}_y)$ for $\alpha_H = 30°$.

Maximum value of $\tilde{\upsilon}_y$ velocity with taking into account pulsation can be with $\tilde{V} \approx 0,84$ and is $\tilde{\upsilon}_y \approx 1,35$.

Maximum value of $\tilde{\upsilon}_y$ with average trust value ($c_T \approx 0{,}01$) is reached with $\tilde{V} \approx 0{,}4$ and it is $\tilde{\upsilon}_y \approx 1{,}25$.

The curve $c_Q / c_{Qh} = f(\tilde{V}_y)$ for $\alpha_H = 30°$ demonstrates that with increase of descent speed c_Q value does not increase.

Vortex ring features partly exist only with $V_Y = 3$ m/s (see Fig. 25, 26). Only front side of 'air body' exists, back side is diffused and 'air body' itself is extremely inclined by flow (see Fig. 25). There are trust and torque coefficients pulsations and also high flapping motions (see Fig. 26).
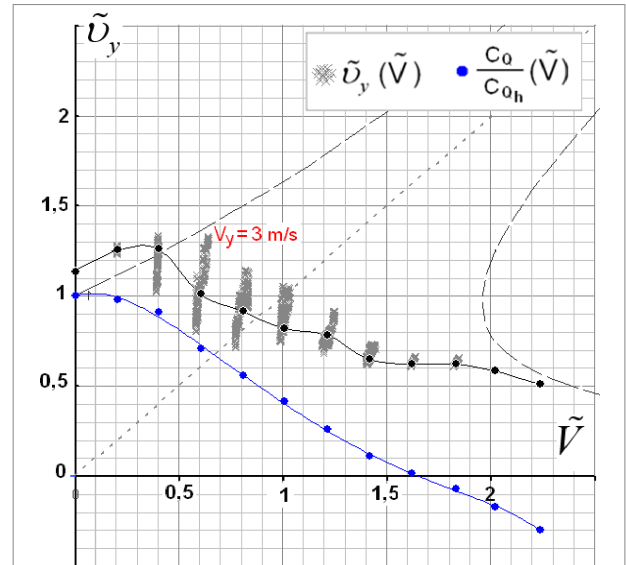

Fig. 24. Diagrams of $\tilde{\upsilon}_y = f\left(\tilde{V}\right)$ and $c_Q / c_{Qh} = f(\tilde{V})$ for $\alpha_H = 30°$.
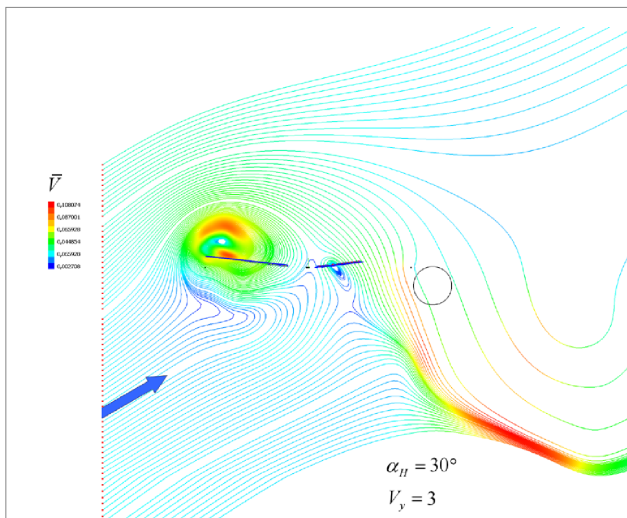

Fig. 25. Airflow lines near main rotor at descent $\alpha_H = 30°$; $V_y = 3$ m/s.
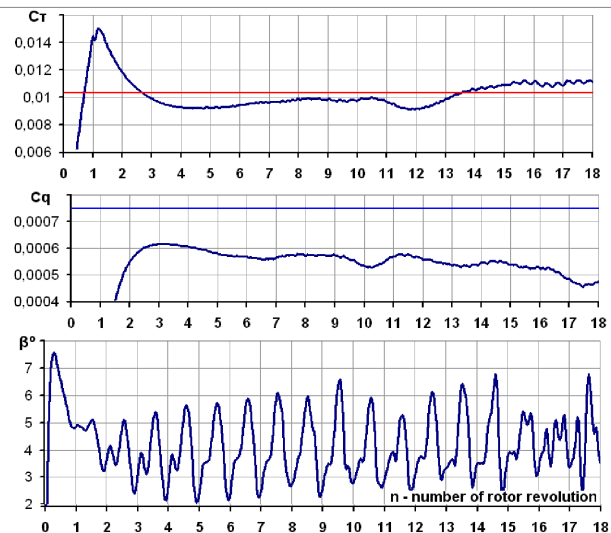

Fig. 26. Airflow lines near main rotor at descent $\alpha_H = 30°$; $V_y = 3$ m/s.

ANALYSIS OF MAIN ROTOR AERODYNAMIC CHARACTERISTICS FOR $\alpha_H = \mathbf{90,70,30°}$

Fig.26 demonstrates summary dependences of $\tilde{\upsilon}_y = f\left(\tilde{V}\right)$ for $\alpha_H = 90,70,30°$. Curves for all flight regimes represent area of values connected with aerodynamic characteristics pulsations. There are major pulsations with $\alpha_H = 90°$ and $\alpha_H = 70°$. Maximum value of $\tilde{\upsilon}_y$ with rotor attack angle moves endwise value of $\tilde{V}$ towards minor values.

Fig. 27 demonstrates summary dependences of $c_Q / c_{Qh} = f(\tilde{V})$ for $\alpha_H = 90,70,30°$. Curves analysis proves that maximum growth of main rotor torque is seen

for $\alpha_H = 90°$ (65%), for $\alpha_H = 70°$ it is significantly lower (17%), and for $\alpha_H = 30°$ there is no torque growth.

Fig. 28 represents the comparison of computational curve of $\tilde{\upsilon}_y = f(\tilde{V})$ (for $\alpha_H = 90°$) with experimental data [3,8,9,10]. In general, satisfactory coincidence is observed. The differences between results received and experimental data prove that rotor aerodynamic characteristics at the vortex ring state modes depend on experimental conditions, determined by Re number, level of air turbulence and also geometric characteristics of rotor (twist, blade number, form in plan).
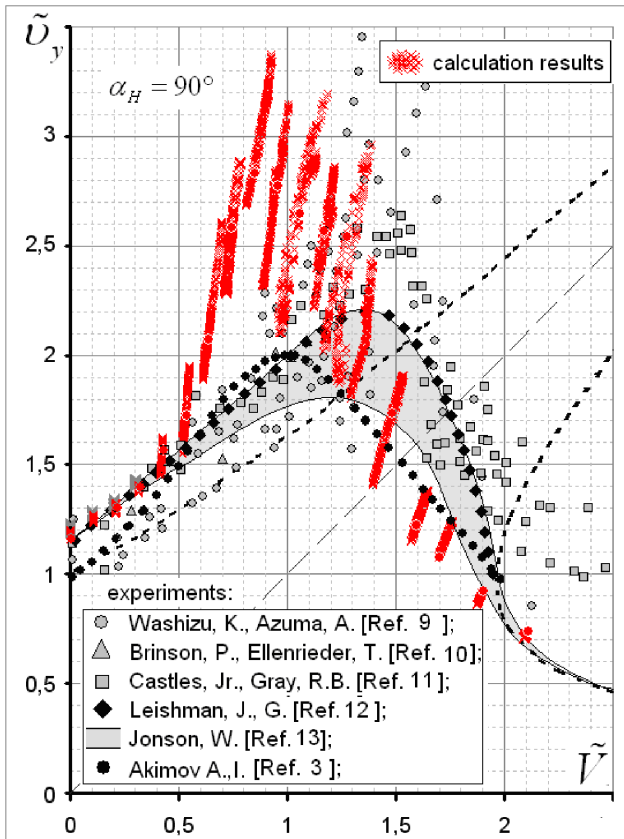

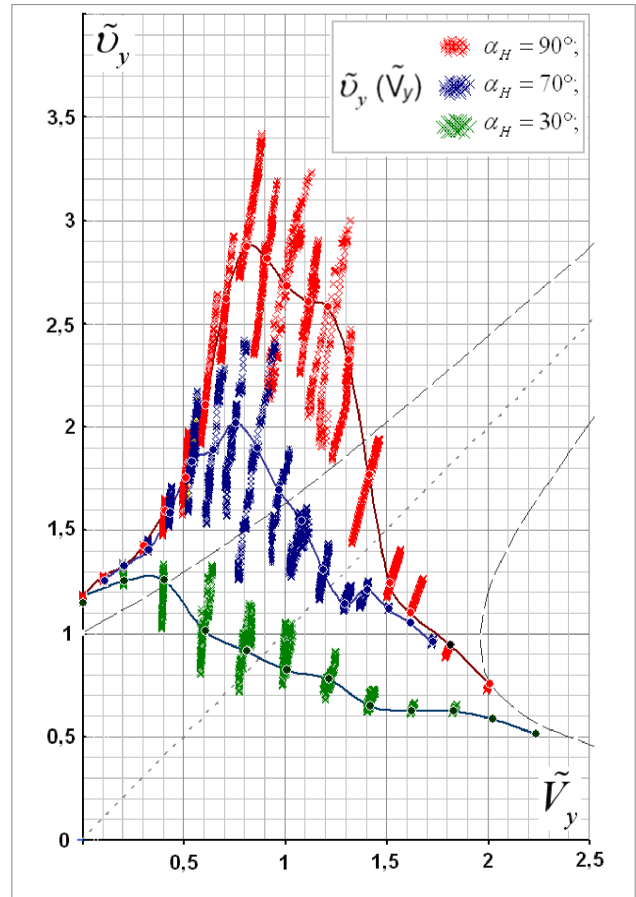**Fig. 29.** Comparison of experimental data with calculation.

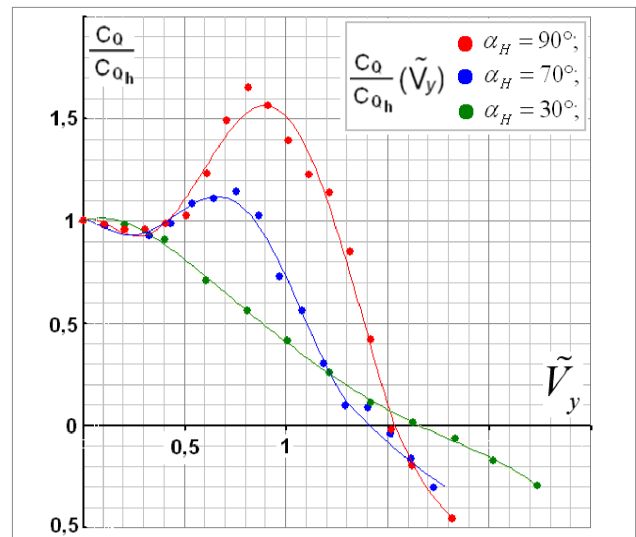**Fig. 27.** Diagram of $\tilde{\upsilon}_y = f(\tilde{V})$.

Fig. 28. Diagram of $c_Q / c_{Qh} = f(\tilde{V})$.

COMPUTER MODELING OF MAIN
AND TAIL ROTOR INTERFERENCE
AT THE VORTEX RING STATE MODE
OF MAIN ROTOR

As it was pointed out before, forming of air body with upper and lower borders is one of the basic peculiarities of main rotor flowing at the vortex ring state mode. This process at the vortex ring state mode is circulating (see Fig. 7, 8, 16, 17), that's why vortex wake is not taken away by airflow, but is accumulated near rotor disk plane. At these modes there is more interference between main and tail rotors, because tail rotor is located near the core of main vortex ring.

Changes in main rotor characteristics influence its effectiveness in anti-torque work and helicopter control. Also it is necessary to take into account the fact of torque value significant increase at the vortex ring state mode. Mostly this increase is typical for vertical descent ($\alpha_H = 90°$) (see Fig. 8).

Flowing analysis of main rotor at the vortex ring state mode demonstrates a case when tail rotor moves into vortex ring core in cross section. In this case velocity field which is caused by vortex ring highly influences tail rotor (see Fig 30).

Circulating airflow being put over rotary axis speed is added to it or subtracted, increasing or decreasing rotation speed of tail rotor – and this depends on its rotation direction (see Fig. 30, 31).

To study this problem main and tail rotors aerodynamics was modeled taking into account their mutual interference. Helicopter descent with $V_Y = 8$ m/s and $\alpha_H = 90°$ for two types of rotation directions (CW and CCW) was studied (see Fig. 31).

Fig. 32 demonstrates calculating curves of tail rotor trust during the time for CW and CCW rotation.

The graphs show that different rotation direction of tail rotor for its work with main rotor at the vortex ring state mode results in different values of its trust.

Maximum difference in tail rotor trust due to different rotation direction in this case reaches up to 25%.
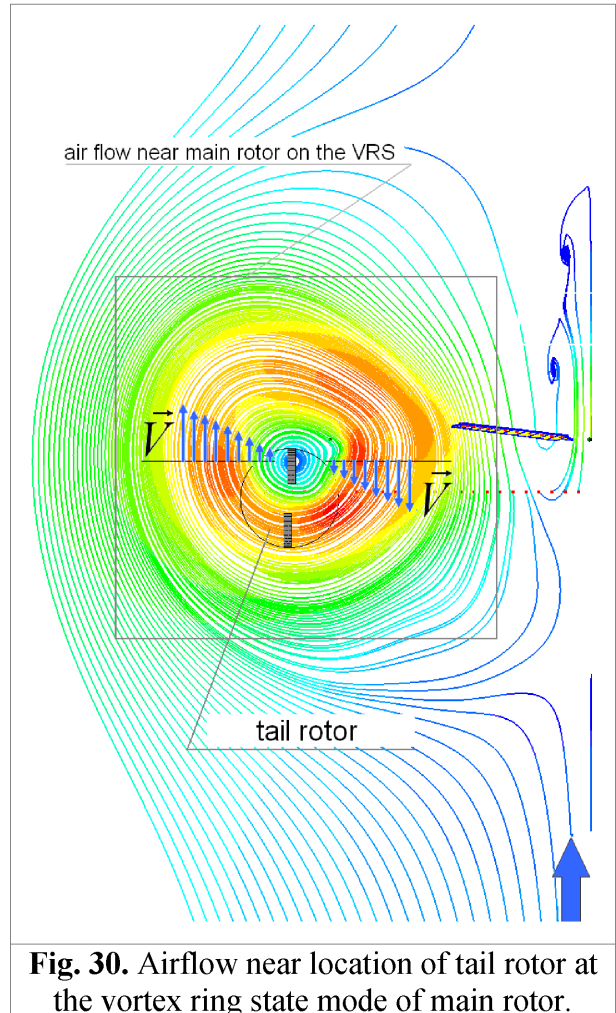

Fig. 30. Airflow near location of tail rotor at the vortex ring state mode of main rotor.
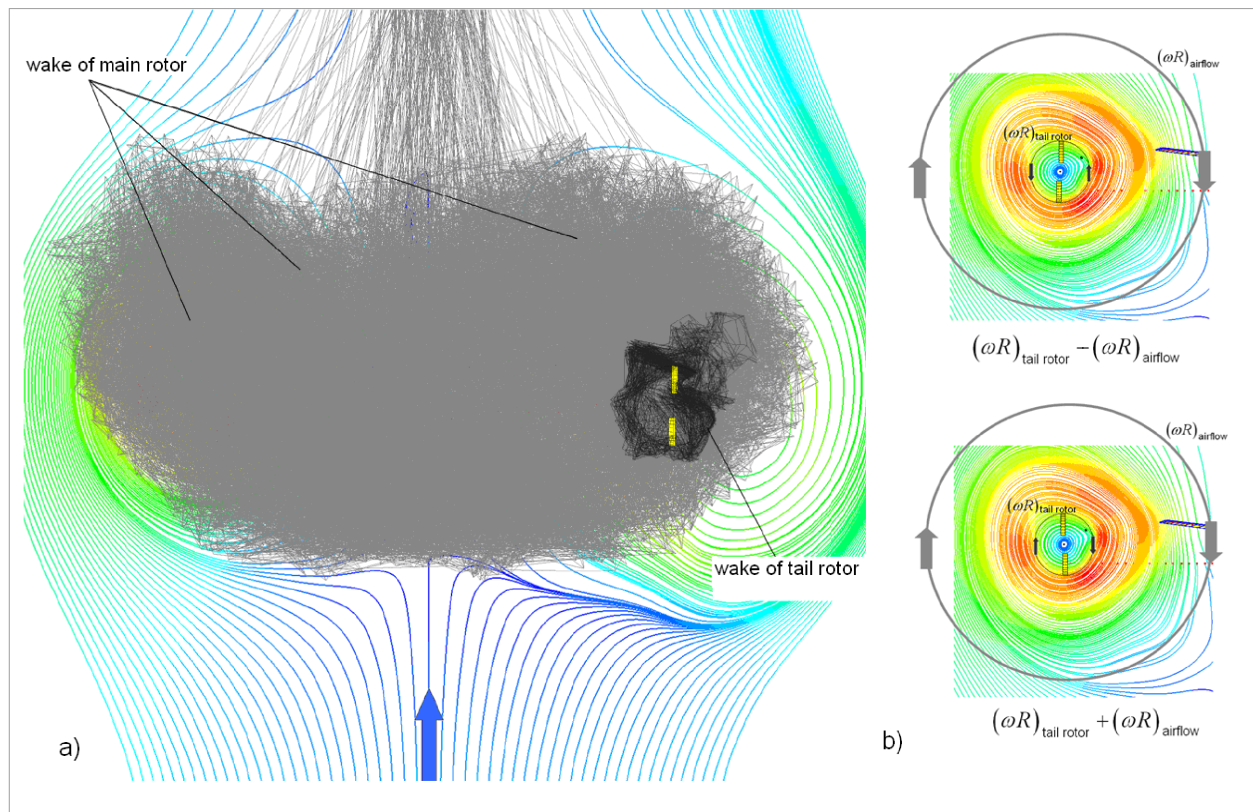
Fig. 31.
a) Main and tail rotors vortex wake with taking into account their interference;
b) Increase and decrease of rotary axis speed (ωR) of tail rotor due to flow near vortex ring core at the vortex ring state mode of main rotor.
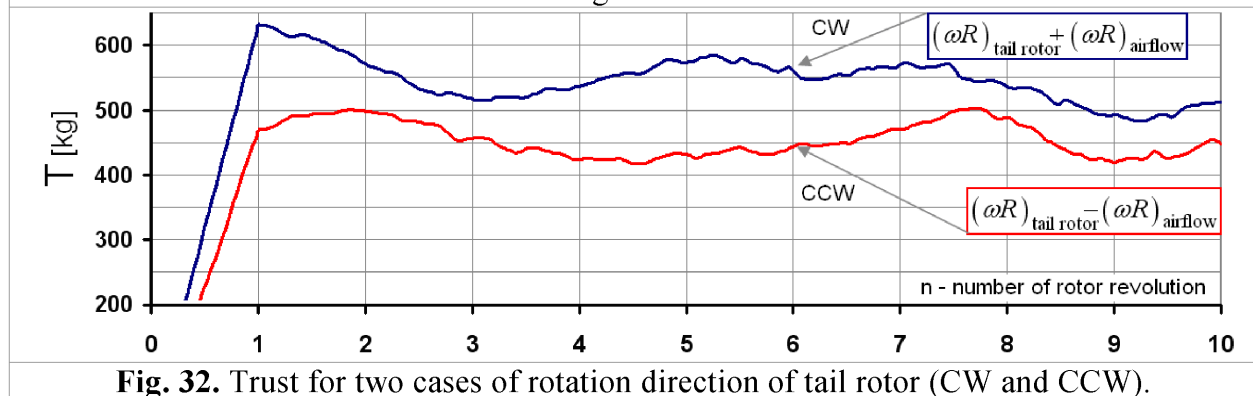

Fig. 32. Trust for two cases of rotation direction of tail rotor (CW and CCW).

SUMMARY

Non-linear blade vortical model (free-wake model) used in the paper allows to model rotor aerodynamics and to calculate its aerodynamic characteristics at the whole range of flight regimes including vortex ring state mode area.

Computational modeling allowed getting the visualization of rotor flown by airflow, peculiarities of total aerodynamic characteristics changes, values of aerodynamic loads on the rotor and their pulsation.

Comparison of received results with available data of experimental and flight tests demonstrated their satisfactory coincidence proving sufficient accuracy of the method used.

Analyzing received results it becomes possible to identify the borders of such dangerous and complicated regime as vortex ring state mode and to analyze its different

peculiarities for a concrete rotor without using of expensive experiments or dangerous flight tests.

Combined modeling of main and tail rotors for classical single rotor scheme of helicopter allowed evaluating vortex wake impact on tail rotor by main rotor.

Calculation results demonstrated that rotation direction of tail rotor CCW, when its rotary axis speed decreases due to the impact of flow near vortex ring core at the vortex ring state mode of main rotor, is irrational.

Significant decrease of tail rotor trust reduces possibility of main rotor torque compensation. This fact can be especially dangerous taking into account significant increase of main rotor torque at the vortex ring state mode.

REFERENCE:
1. Ignatkin Y. M., Makeyev P. V., Grevtsov B. S., Shomov A. I. A nonlinear blade vortex propeller theory and its applications to estimate aerodynamic characteristics for helicopter main rotor and anti-torque rotor. Vestnik MAI, № 5, 2009, v. 16 (in Russian).
2. Ignatkin Y. M., Makeyev P. V., Shomov A. I. Researches of aerodynamic characteristics of helicopter rotor on vortex ring state mode by nonlinear blade vortex model. Vestnik MAI, № 6, 2009, v. 16 (in Russian).
3. Akimov A.I. Aerodynamics and flight characteristics of helicopters. Moscow, Engineering, 1988 (in Russian).
4. Brown, R. E., Newman, S. J., Leishman, J. G., and Perry, F. J., "Blade Twist Effects on Rotor Behaviour in the Vortex Ring State," Proceedings of the 28th European Rotorcraft Forum, 2002.
5. Leishman, J. G., Bhagwat, M. J., and Ananthan, S., "Free-Vortex Wake Predictions of the Vortex Ring State for Single Rotor and Multi-Rotor Configurations," Proceedings of the 58th Annual Forum of the American Helicopter Society International, Montr´eal Canada, 2002.
6. Leishman, J. G., Bhagwat, M. J., and Ananthan, S., "Free-Vortex Wake Predictions of the Vortex Ring State for Single Rotor and Multi-Rotor Configurations," Proceedings of the 58th Annual Forum of the American Helicopter Society International, Montr´eal Canada, 2002.
7. R. Celi, M. Ribera. Time Marching Simulation Modeling in Axial Descending Through the Vortex Ring State. 63rd American Helicopter Society International Annual Forum 2007
8. Newman, S. J., Brown, R., Perry, J., Lewis, S., Orchard, M., and Modha, A., "Comparative Numerical and Experimental Investigations of the Vortex Ring Phenomenon in Rotorcraft," Proceedings of the 57th Annual Forum of the American Helicopter Society International, 2001
9. Washizu, K., Azuma, A., Koo, J., and Oka, T., "Experiments on a Model Helicopter Rotor Operating in the Vortex Ring State," Journal of Aircraft, Vol. 3, No. 3, May-June 1966, pp. 225– 230.
10. Brinson, P., and Ellenrieder, T., Experimental Investigation of Vortex Ring Condition, Proceedings of the 24th European Rotorcraft Forum, Marseilles, France, 1998.
11. Castles, Jr., and Gray, R.B., "Empirical Relation between Induced Velocity, Trust, and Rete of Descent of a Helicopter Rotors as Determined by Wind-Tunnel Tests on Four Model Rotors," NASA TN-2474, October 1951.
12. J. Gordon Leishman. Principles of Helicopter Aerodynamics. Cambridge University Press. 2000.
13. W. Jonson. Helicopter theory. Courier Dover Publications, 1994.
14. Vozhdaev E.S. Helicopter aerodynamics. Engineering. Encyclopedia. Vol. 4041. Airplanes and helicopters. Book 1. Aerodynamics dynamics and strength. Engineering Press, 2002. (in Russian).